

GENERAL ARTICLE

Variants in *USP48* encoding ubiquitin hydrolase are associated with autosomal dominant non-syndromic hereditary hearing loss

Sissy Bassani^{1,2}, Edward van Beelen³, Mireille Rossel⁴, Norine Voisin¹, Anna Morgan⁵, Yoan Arribat⁶, Nicolas Chatron^{1,7}, Jacqueline Chrast¹, Massimiliano Cocca⁵, Benjamin Delprat⁴, Flavio Faletra⁵, Giuliana Giannuzzi^{1,†}, Nicolas Guex⁸, Roxane Machavoine⁹, Sylvain Pradervand¹, Jeroen J. Smits¹⁰, Jiddeke M. van de Kamp¹¹, Alban Ziegler⁹, Francesca Amati⁶, Sandrine Marlin⁹, Hannie Kremer¹⁰, Heiko Locher³, Tanguy Maurice⁴, Paolo Gasparini^{2,5}, Giorgia Giroto^{2,5} and Alexandre Reymond^{1,*}

¹Center for Integrative Genomics, University of Lausanne, Lausanne, Switzerland, ²Department of Medicine, Surgery and Health Sciences, University of Trieste, Trieste, Italy, ³Department of Otorhinolaryngology, Leiden University Medical Center, Leiden, The Netherlands, ⁴MMDN, Univ Montpellier, EPHE, INSERM, Montpellier, France, ⁵Institute for Maternal and Child Health, IRCCS, Burlo Garofolo, Trieste, Italy, ⁶Department of Biomedical Sciences, University of Lausanne, Lausanne, Switzerland, ⁷Service de Génétique, Hospices Civils de Lyon, Lyon, France, ⁸Bioinformatics Competence Center, University of Lausanne, Lausanne, Switzerland, ⁹Centre de référence Surdités Génétiques, Hôpital Necker, Institut Imagine, Paris, France, ¹⁰Hearing and Genes, Department of Otorhinolaryngology and Department of Human Genetics, Donders Institute for Brain, Cognition and Behaviour, Radboud University Medical Center, Nijmegen, The Netherlands and ¹¹Department of Clinical Genetics, Amsterdam UMC, Vrije Universiteit Amsterdam, Amsterdam, The Netherlands

*To whom correspondence should be addressed at: Center for Integrative Genomics, Genopode Building, University of Lausanne, CH-1015 Lausanne, Switzerland. Tel: +41 21 692 3930; Fax: +41 21 692 3965; Email: alexandre.reymond@unil.ch

Abstract

Non-Syndromic Hereditary Hearing Loss (NSHL) is a genetically heterogeneous sensory disorder with about 120 genes already associated. Through exome sequencing (ES) and data aggregation, we identified a family with six affected individuals and one unrelated NSHL patient with predicted-to-be deleterious missense variants in *USP48*. We also uncovered an eighth patient presenting unilateral cochlear nerve aplasia and a *de novo* splice variant in the same gene. *USP48* encodes a ubiquitin carboxyl-terminal hydrolase under evolutionary constraint. Pathogenicity of the variants is supported by *in vitro* assays that showed that the mutated proteins are unable to hydrolyze tetra-ubiquitin. Correspondingly, three-dimensional representation of the protein containing the familial missense variant is situated in a loop that might

[†] Present address: Department of Biosciences, University of Milan, 20133 Milan, Italy; Institute of Biomedical Technologies, National Research Council (CNR), 20054 Segrate, Italy.

Received: April 29, 2021. Revised: May 25, 2021. Accepted: May 25, 2021

© The Author(s) 2021. Published by Oxford University Press. All rights reserved. For Permissions, please email: journals.permissions@oup.com

influence the binding to ubiquitin. Consistent with a contribution of *USP48* to auditory function, immunohistology showed that the encoded protein is expressed in the developing human inner ear, specifically in the spiral ganglion neurons, outer sulcus, interdental cells of the spiral limbus, stria vascularis, Reissner's membrane and in the transient Kolliker's organ that is essential for auditory development. Engineered zebrafish knocked-down for *usp48*, the *USP48* ortholog, presented with a delayed development of primary motor neurons, less developed statoacoustic neurons innervating the ears, decreased swimming velocity and circling swimming behavior indicative of vestibular dysfunction and hearing impairment. Corroboratingly, acoustic startle response assays revealed a significant decrease of auditory response of zebrafish lacking *usp48* at 600 and 800 Hz wavelengths. In conclusion, we describe a novel autosomal dominant NSHHL gene through a multipronged approach combining ES, animal modeling, immunohistology and molecular assays.

Introduction

Hearing loss is the most common sensory disorder affecting an estimated 6% of the population (WHO—https://www.who.int/health-topics/hearing-loss#tab=tab_1). Approximately 60% of the cases of inherited deafness are due to malfunction of inner ear structures such as the cochlea and the auditory nerve (1). Its hereditary fraction can be divided in syndromic (~30% of cases) and non-syndromic (~70% of cases) forms. Notwithstanding that ~120 genes have already been associated with Non-Syndromic Hereditary Hearing Loss (NSHHL) (2), the current genetic tests fail to provide a diagnosis in almost half of the cases (3). This suggests that many novel deafness genes still need to be characterized.

Zebrafish are becoming a popular model for hearing loss studies due to their rapid development of morphological specializations for hearing. From 5 days post-fertilization (dpf), they detect sound waves (4), allowing researchers to test their auditory capacity through acoustic startle response (ASR) (5). From a genetic point of view, more than 50 genes are known to impact the auditory inner ear and the vestibular system of zebrafish (5), and many of these genes are conserved and associated with the inner ear development and function in other vertebrates, including humans (6,7). These features combined with ease of maintenance and accessibility to the inner ear, make zebrafish an attractive and suitable model to investigate the development and molecular genetics of the vertebrate inner ear.

Members of the ubiquitin-specific proteases family have been associated with hearing loss. Specifically, the catalytically inactive tight junction-associated *Usp53* was shown to be essential for the survival of auditory hair cells and normal hearing in mice (8), while variants in the dog *USP31* were associated with adult-onset deafness in border collies (9). Histological findings further support the involvement of ubiquitin in hearing as ubiquitin-positive granules were identified in the neuropil of cochlear nuclei of aging dogs (10). In this study, we combined exome sequencing (ES), data aggregation from multiple laboratories, animal modeling and molecular assays to associate *USP48* (MIM: 617445) variants with an autosomal dominant NSHHL (ADNSHHL). Intriguingly, both *USP31* and *USP48* regulate the nuclear factor- κ B (11), whose deficiency was associated with auditory nerve degeneration and increased noise-induced hearing loss (12).

Results

Within our NSHHL Italian families, we analyzed a four-generation family with six affected individuals (Fig. 1A; Supplementary Material Fig. S1). The proband (IV:2) presented with slight (low frequency) to severe (mid- to high frequencies)

bilateral sensorineural hearing loss and was first diagnosed at 8 years of age. He is using hearing aids since. Tympanometry revealed a tympanogram type A. While otoacoustic emissions have not been tested, clinical evaluation showed no motor or vestibular problems. CT, MRI, an ophthalmological evaluation and a thyroid and dysmorphological assessments resulted normal. Her mother (III:2) presented moderate (mid-frequencies) to slight (high frequencies) bilateral sensorineural hearing loss, whereas her maternal uncle (III:1) showed severe (low frequencies) to profound (mid- to high frequencies) bilateral sensorineural hearing loss. Hearing loss requiring prosthesis was diagnosed in the maternal grandmother (II:2) at 50 years of age. She showed moderate (low frequencies) to severe (mid-frequencies) to profound (high frequencies) bilateral sensorineural hearing loss. Her brother (II:3) is affected by severe hearing loss across all frequencies with his left ear reaching a moderate loss at 4 kHz. His deafness was recognized at birth and worsened in adulthood (Fig. 1A; Supplementary Material, Fig. S1).

As targeted screening of the commonest 99 deafness genes in the affected subjects was negative, the affected individuals IV:2, III:1, III:2 and II:3, as well as the unaffected members IV:1 and III:3 of the family (Fig. 1 and B) were subjected to ES. These analyses showed that no rare variant segregated with the disease made exception of a missense variant in *USP48* NC_000001.10:g.22056281C>T, NM_032234.7:c.1216G>A, NP_115612.4:p.(Gly406Arg) (GRCh37/hg19) (Fig. 1A and B). While it is predicted to be deleterious by multiple prediction tools (PolyPhen-2: possibly damaging, score=1; SIFT: deleterious, CADD=29.1, GERP=5.44), this variant is present in GnomAD v2.1.1 with a minor allele frequency (MAF) of 6.7×10^{-5} (17 allele out of 251304 with no homozygotes). Consistent with the presence of this variant in supposedly healthy individuals, we observed an incomplete penetrance of the disease within our family, with one hearing individual (III:4) heterozygote for this variant (Fig. 1A and B). His most recent audiometric evaluation was performed in 2019 at 39 years of age (Supplementary Material, Fig. S1). This is consistent with the notion that many of the developmental disorder genes awaiting discovery are likely to be less penetrant than the currently known genes (13). Note also that while GnomAD 'has made every effort to exclude individuals with severe pediatric diseases, they do not rule out the possibility that some of their participants do actually suffer from a disease of interest'. No other rare variant segregated with the disease.

USP48 is expressed in the human cerebellum and cerebellar hemisphere (The Human Protein ATLAS; Genome Browser) and in the cochlear and vestibular sensory hair cells of mice and zebrafish (gEAR Portal 2020). It is often somatically mutated in the pituitary adenomas, i.e. Cushing's disease (14,15). This gene is under evolutionary constraint with five observed loss of

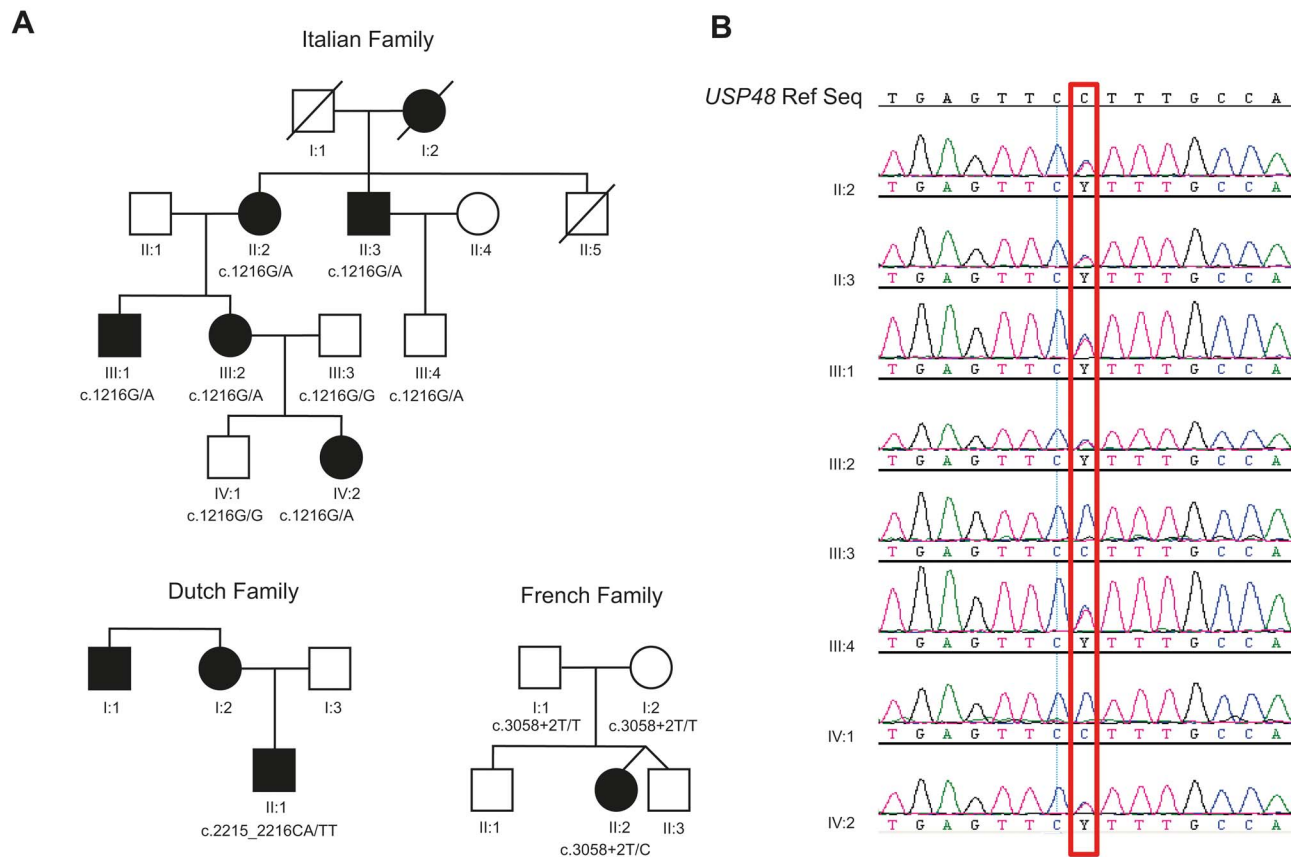


Figure 1. Pedigrees and Sanger sequencing. (A) Pedigree of the Italian family carrying the (c.1216G/A) variant in *USP48* (top). Pedigrees of the Dutch presenting the variant (c.2215_2216delinsTT) and French family carrying the variant (c.3058 + 2 T > C) in *USP48* (bottom left and right, respectively). Filled symbols represent affected individuals. (B) Sanger sequencing traces confirming the segregation of variant (c.1216G/A) in the Italian family.

function variants (LoF, i.e. truncation variant) versus 65 expected (ratio $o/e = 0.08$ [0.04–0.16]; pLI (probability of LoF intolerance) = 1) and 256 observed missense variants versus 548 expected ($o/e = 0.47$ [0.42–0.52]; $Z = 4.37$) in GnomAD. Whereas intolerance to truncating variants is customarily used to narrow down lists of causative variants in autosomal dominant intellectual disability and syndromic developmental disease, we wondered if this was a good selection criterion when searching for genes associated with autosomal dominant NSHL (ADNSHL). To evaluate this criterion, we assessed the distribution of o/e LoF ratio of the 46 known ADNSHL genes (Supplementary Material, Table S1). While some ADNSHL genes are not constrained especially the prevalent ones (e.g. *GJB2* $o/e = 2.62$ and *GJB6* $o/e = 1.07$), we observed that 30 out of 46 ADNSHL genes (65%) present with an o/e LoF ratio below 0.5. This result suggests that the majority of dominant non-syndromic deafness genes are under evolutionary pressure (o/e median = 0.37; Fig. 2C) and that this can be used as a selection criterion upon screening for novel rare ADNSHL causative genes. Of note, *USP48* belongs to the list of genes enriched in ‘brain-critical exons’ that are often prioritized in genotype–phenotype studies of neurodevelopmental conditions (16).

Our search for more cases led to the identification of one Dutch NSHL affected individual who presented with progressive hearing loss starting at 24 years of age without additional syndromic features. At 40 years of age his audiogram, displayed moderate to severe sensorineural hearing loss at all frequencies with asymmetry between both ears. A computed

tomography of the bilateral temporal bones did not show abnormalities.

ES of this patient identified a predicted-to-be deleterious missense variant in *USP48* NC_000001.10:g.22032676_22032677 delinsAA, NM_032236.7:c.2215_2216delinsTT, NP_115612.4:p.(Thr739Leu) (CADD = 23.3; GnomAD MAF = 6.3×10^{-5}). His mother complained of hearing loss since the age of 27 years that progressed to profound hearing loss. A maternal uncle was similarly reported to be hearing impaired. Whereas such a pedigree suggests autosomal dominant inheritance of hearing impairment, as the mother and maternal uncle did not consent samples, we were not able to confirm transmission (Fig. 1A).

We uncovered an eighth affected individual in France presenting with right profound sensorineural hearing impairment diagnosed at 12 months, while left hearing was still normal during the last clinical genetic consultation (at 6 years old). Suggestive of a right cochlear nerve aplasia or hypoplasia, MRI of cerebral and internal auditory canals could not visualize the right cochlear nerve. Temporal bone CT scan was normal. This patient is heterozygote for a *de novo* splice variant in *USP48* (NC_000001.10:g.22013682A > G, NM_032236.7:c.3058 + 2 T > C, NP_115612.4:p.?.; GnomAD MAF = 0) (Fig. 1A). This variant abolishes the donor site according to MaxEntScan, NNSplice and SpliceAI (score = 0.97). This would result in a frameshift meaning that either the encoded RNA would be recognized by nonsense mediated decay (NMD) and degraded, or it will encode a truncated protein, which we showed has lost its enzymatic activity (Fig. 2D). These splice predictors also suggest that the

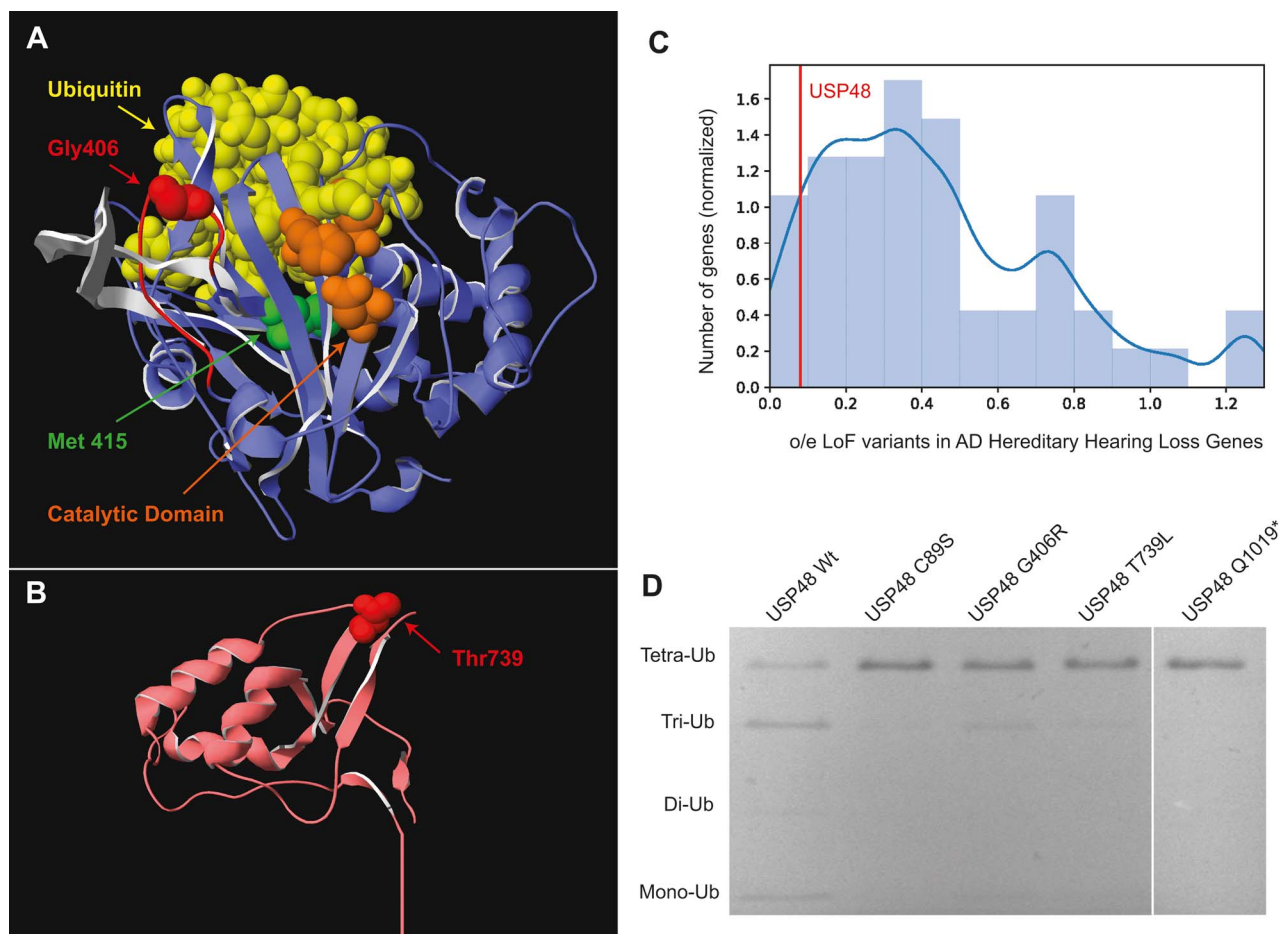


Figure 2. 3D modeling and in vitro functional analysis. (A) USP48 tridimensional protein modeling based on the paralogous USP7 template (blue ribbon). In the model are highlighted the Ubiquitin molecule (yellow), Gly406 mutated in the Italian family (red space-filled residue) within the unstructured loop of residues Tyr498-Asn512 (red ribbon), the equivalent USP9X region bearing residues Phe1921-Asn1947, which form an antiparallel beta-sheet (white ribbon), Met415 mutated in Cushing's disease (green space-filled), three USP48 residues Cys98, His353 and Asn370 of the catalytic triad corresponding to USP7 residues Cys223, His464 and Asp481 (orange space-filled). (B) USP48 tridimensional protein modeling of the DUSP domain (salmon ribbon) highlighting the solvent exposed position of Thr739 (red space-filled) that is mutated in Dutch proband. (C) Whereas intolerance to truncating variants is customarily used to narrow down lists of causative variants in autosomal dominant intellectual disability and syndromic developmental disease we assessed if this was a good selection criterion when searching for genes associated with ADNSHHL. To evaluate this criterion, we assessed the distribution of observed over expected (*o/e*) LoF variants in GnomAD v2.1.1 ($n = 46$ genes, bin width = 0.1). The density distribution and the data normalization have been performed through the Kernel density estimation function. While some ADNSHHL genes are not constrained especially the prevalent ones (e.g. *GJB2* *o/e* = 2.62 and *GJB6* *o/e* = 1.07), we observed that 30 out of 46 ADNSHHL genes (65%) present with an *o/e* LoF ratio below 0.5. This result suggests that the majority of dominant non-syndromic deafness genes are under evolutionary pressure (*o/e* median = 0.37) and that this can be used as a selection criterion upon screening for novel rare ADNSHHL causative genes. The *o/e* ratio of USP48 is indicated with a red line. (D) Ability of the USP48 alleles to hydrolyze tetra-ubiquitin molecules in tri-, di- and mono-ubiquitin molecules. Ubiquitin multimers are separated by SDS-PAGE after incubation with the USP48 enzyme (FLAG-USP48 Wt, FLAG-USP48^{G98S} catalytically dead, FLAG-USP48^{G406R}, FLAG-USP48^{T739L} and FLAG-USP48¹⁻¹⁰¹⁹) mentioned on top of each lane. Please note that whereas FLAG-USP48 Wt is capable of hydrolyzing tetra-ubiquitin (48kD band), the multiple variants identified in the patients and the catalytically dead variant are impaired. While some intermediate polyubiquitin bands are nevertheless visible in the corresponding lanes, it is not possible to distinguish if these results are due to passive degradation of tetra-ubiquitin or residual enzymatic activity of the variants.

next GT will not be used because of a unfavorable preceding TTT stretch, which should result in the addition of 10 new residues before a TGA opal stop codon p.(Val1020Glyext*9). While we cannot exclude that the association between the French patient and USP48 is spurious before identification of other similarly affected individuals, we think that it is important to document this case.

USP48 encodes a ubiquitin carboxyl-terminal hydrolase able to recognize and hydrolyze the Glycine or Lysine peptide bond at the carboxy-terminus of ubiquitin. While the amino-terminus of USP48 contains the ubiquitin carboxyl-terminal hydrolase domain (residues 86–457), its C-terminal part comprises three sequential DUSP (domain present in ubiquitin-specific

proteases) from residues 465–548, 571–686 and 714–1004. DUSPs are present in other ubiquitin-specific proteases, such as USP4, USP11 and USP15, and help them determine their biological activity and specificity of binding (17). For example, the DUSP-Ubl domain of USP4 was shown to be necessary to enhance ubiquitin dissociation and achieve full catalytic turnover (18). The pathogenicity of the Italian variant is supported by the three-dimensional representation of the encoded peptide. The mutated residue is located within a flexible loop that flanks over the catalytic site of the hydrolase and could play a role in substrate specificity (Fig. 2A). Of note the Met415 residue, often found somatically mutated in Cushing's disease, i.e. adenomas of the pituitary (14,15), is only a few residues after the end

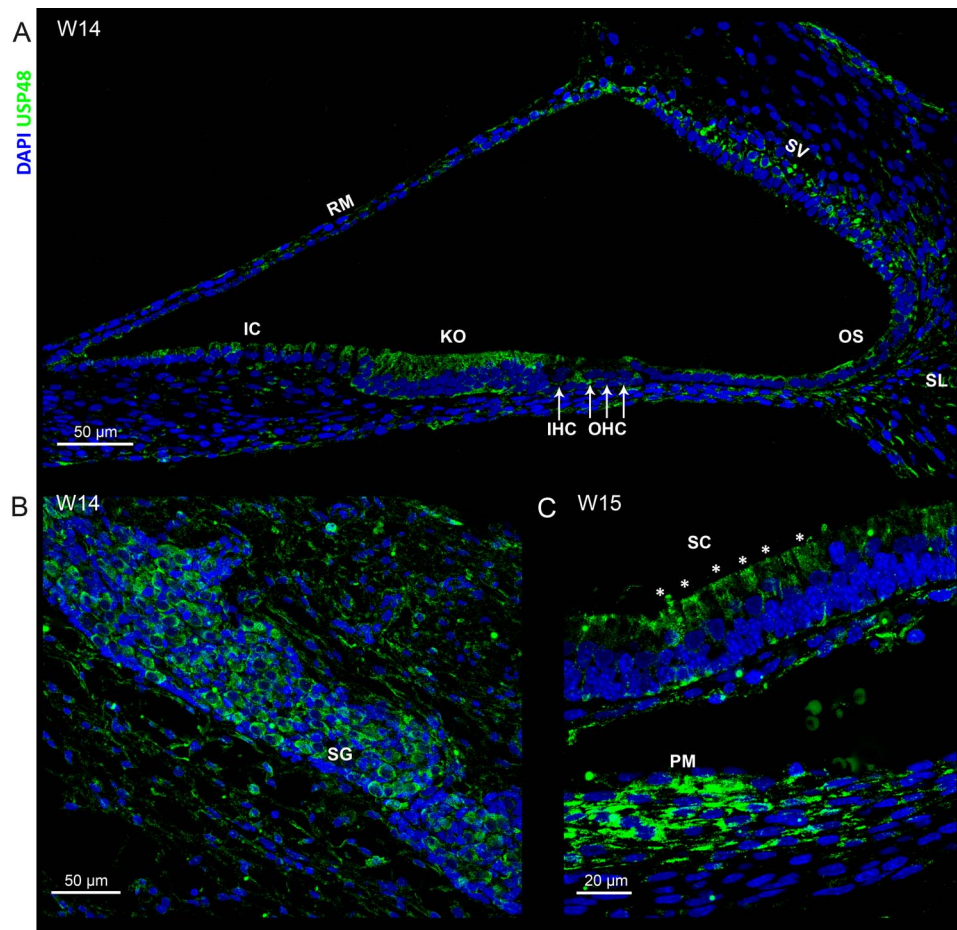


Figure 3. USP48 expression in the human fetal inner ear. Human embryonic ear immunostaining showing DNA (DAPI) in blue and the USP48 protein in green. USP48 is expressed in several structures: (A) at W14, in Kolliker's Organ, the OS, the fibrocytes of the SL, the interdental cells of the spiral limbus (IC), the intermediate cells of the SV and in RM, but not in the IHCs or OHCs; (B) at W14, in the neurons and supporting mesenchyme of the SG; (C) at W15 in the PM and the SCs of the saccule macula of the vestibular system (pinpointed by asterisks).

of the loop bearing Gly406, in a stretch of residues [AYMLVY] conserved in USP48 orthologs and in a region positioned close to ubiquitin ($<8 \text{ \AA}$) and within 12 \AA of active site residues Cys98 and His353 (Fig. 2A). The Thr739, residue mutated in the Dutch patient, is situated in a conserved T-D-[VE]-L-Y stretch found in 185 Swiss-Prot sequences. A search for templates using HHPRED (19) identified a DUSP (domain present in USPs) fold (pdb entry 3LMN; DOI 10.2210/pdb3LMN/pdb). NetPhos 3.1 (20) predicts that Thr739 could be phosphorylated by CKII or an unspecified kinase (score of 0.508 and 0.755, respectively), whereas Src could be phosphorylating the neighboring Tyr743 (0.505). These kinases have been identified in a screen for enzymes involved in ototoxic damage to the murine organ of Corti (21). Mutation of this threonine residue could affect phosphorylation status and protein-protein interaction as it is exposed on the surface of the DUSP domain (Fig. 2B).

We then assessed *in vitro* the effect of the USP48 variants on the activity of the encoded ubiquitin carboxyl-terminal hydrolase. The peptides FLAG-USP48^{WT} (wild-type), FLAG-USP48^{C98S}, encoding a catalytically dead enzyme, FLAG-USP48^{G406R}, FLAG-USP48^{T739L} and FLAG-USP48¹⁻¹⁰¹⁹ that encodes only the first 1019 amino-terminal residues of the protein and mimics the French variant, were expressed in HEK293T cells. We assessed the ability of the corresponding anti-FLAG immunoprecipitated extracts to

hydrolyze ubiquitin upon incubation with tetra-ubiquitin. We observed that like the catalytically dead enzyme and contrary to the wild-type molecule, the truncated USP48 hydrolase and the ones containing the ADNSHHL missense variants identified in the Italian and Dutch affected individuals showed an impaired ability to cleave tetra-ubiquitin into tri-, di- and mono-ubiquitin (Fig. 2D).

Consistent with a contribution of USP48 to auditory function and according to the gear portal, the orthologous transcript is found in different types of cells of P1 mouse cochlear epithelium. Using immunohistology, we then showed that the human USP48 protein is present in fetal inner ear specimens. In inner ears of W12- and W14-old human fetuses, we found antigens recognized by anti-USP48 antibodies in the cytoplasm of supporting cells (SCs) within the Kolliker's organ, the earliest epithelial structure present in the developing auditory sensory organ (22), in interdental cells, in cells of the outer sulcus (OS), in the Reissner's membrane (RM) and in fibrocytes of the spiral ligament (SL, Fig. 3A). Transient expression was observed in intermediate cells of the stria vascularis (SV) at W14 (Fig. 3A), but not at W12 (Supplementary Material, Fig. S2A). Spiral ganglion (SG) neurons and the surrounding mesenchyme also expressed USP48 (Fig. 3B). In addition, USP48 is present in the vestibular system, in particular in SCs of the saccular macula and ampulla,

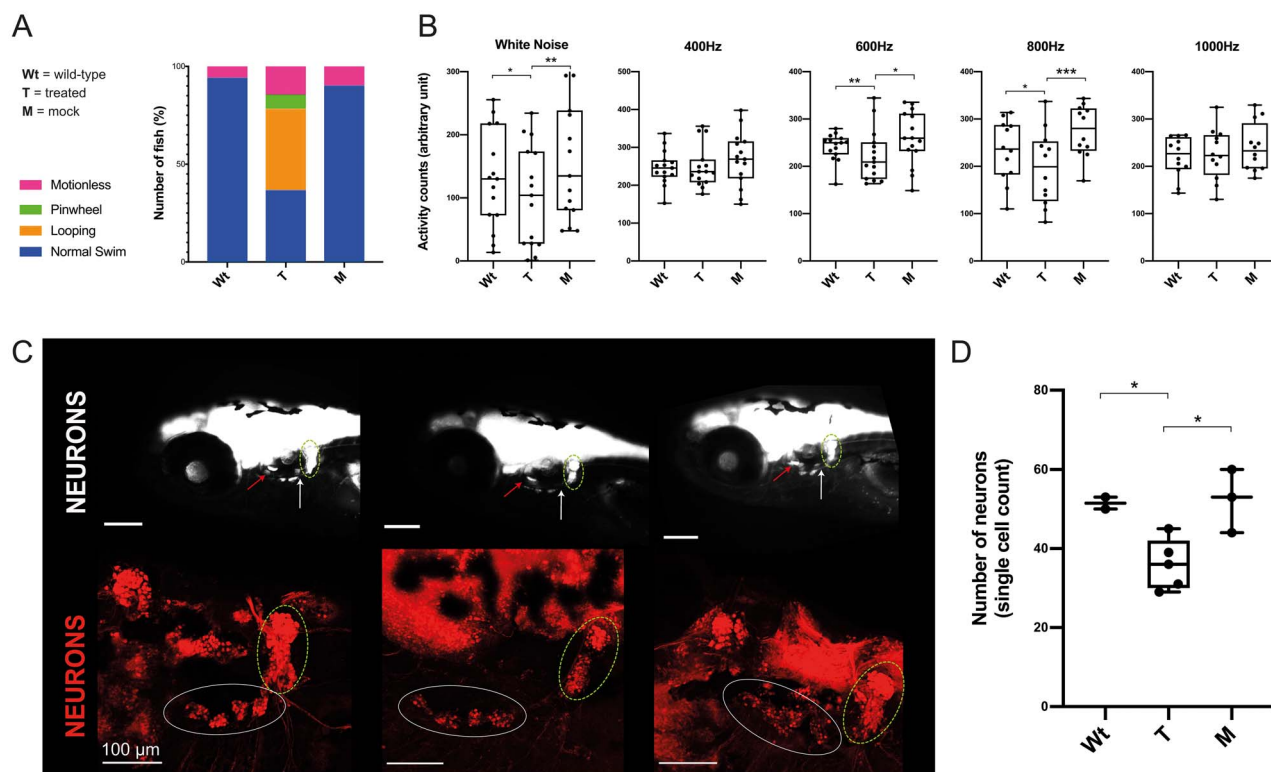


Figure 4. *usp48* knocked-down zebrafish model. (A) Touch Test Response of 3 dpf wild-type (Wt; $n = 71$), *usp48* knocked-down (*usp48-4* + Cas9; treated:T; $n = 41$) and control zebrafish (*usp48-4*; mock:M; $n = 32$). (B) Acoustic Startle Response of 5 dpf wild-type (Wt; $n > 40$), *usp48* knocked-down (*usp48-4* + Cas9; treated:T; $n > 40$) and controls zebrafish (*usp48-4*; mock:M; $n > 40$) toward white noise (broad-band noise), 400, 600, 800 and 1000 Hz lengths. (C) Maximum projections of confocal images regarding specific neuronal structures in 5 dpf Wt, T and M fish: the statoacoustic neurons (red arrows), Xth ganglia (white arrows) and the posterior lateral line ganglia (green ellipses) are indicated in the top panels; the statoacoustic neurons and PPLG are pinpointed with white and green ellipses, respectively, in the bottom panels. (D) Number of statoacoustic neurons (single cell count) in 5 dpf Wt ($n = 2$), T ($n = 5$) and M ($n = 3$) fish. P-value legend: * ≤ 0.02 .

the periotic mesenchyme (PM), the neuronal cell bodies of the Scarpa's ganglion and the epithelial cells of the semicircular canals of W15 embryos (Fig. 3C, Supplementary Material, Fig. S2B and C). No expression was seen in the inner or outer hair cells (OHCs) of the cochlea and in the hair cells of the vestibular system at these developmental stages.

To gain insight into the function of USP48, we ablated the orthologous *usp48* in zebrafish by CRISPR/Cas9 genome editing (23). While a knock-in of one of the missense variants would have more accurately modeled the affected individuals, the engineered knock-down still mimics the decrease in ubiquitin carboxyl-terminal hydrolase enzymatic activity observed in our *in vitro* assays and the truncation variant. We engineered F0 larvae using three different small guide RNAs targeting exons 4 (*usp48-4*), 9 and 10 of *usp48* and assessed their locomotion and touch response. Swimming in circle upon touching was suggested to be an indicator of vestibular dysfunction and auditory impairment (24). At 3 dpf, we observed that an increased fraction of crispant animals swam in circle in response to a tactile stimulus compared with wild-type and mock-treated fish (Fig. 4A). Similarly, 5 dpf mutant larval batches showed a reduction in both global velocity and net speed (Supplementary Material, Fig. S4). The *usp48* targeting exon 4 appeared as the most efficient guide with notable effects on global velocity (*usp48-4* + Cas9 (treated) 1.0 versus *usp48-4* (mock-treated controls) 1.4 mm/s; $P = 0.04$), net speed (5.4 versus 6.1 mm/s; $P = 0.01$) and tactile response assays (78 versus 12% miss-responding) (Fig. 4A, Supplementary Material, Fig. S4). We

assessed the presence of microdeletion and showed that *usp48-4* induced genetic editing in 75% of injected embryos (founders, F0). We then tested the auditory startled responses of *usp48* mutant larvae at 5 dpf. Consistent with hearing impairment, they presented with a significantly decreased response to white noise ($P = 0.05$; Fig. 4B). Upon stratifying by frequency, we found that *usp48* knocked-down fish larvae presented with a significantly decreased reaction when compared with wild-type and mock-treated fish toward 600 ($P = 0.03$) and 800 Hz ($P = 0.0017$) pulses but not to the shorter 400 Hz ($P = 0.18$) and longer 1000 Hz ($P = 0.16$) frequencies (Fig. 4B). This impaired response to acoustic cues was not complemented by changes in the response to light as we observed no significant differences in the visual motor response (VMR) of *usp48* knocked-down, wild-type and mock-treated fish larvae during light-dark transitions (Supplementary Material, Fig. S5). To possibly uncover the origin of this hearing impairment, we first analyzed the development of sensory hair cells of *usp48* knocked-down zebrafish. We investigated both AB-line zebrafish dyed with YO-PRO-1 that selectively labels neuromast hair cells and Brn3c: mGFP/NBT:dsRED zebrafish whose hair cells of the inner ear and lateral line neuromasts are labeled green, while neurons are stained in red. The superficial sensory hair cells of *usp48* knocked-down fish showed a normal mechano-transduction function and the neuromasts presented a regular superficial distribution along the anterior (head) and posterior (trunk and tail) lateral-line systems (Supplementary Material, Fig. S6). We then assessed the development of the neuronal system and discovered that the vestibulo-acoustic

neurons innervating the ear bases were less developed in 5 dpf *usp48* knocked-down than in mock-treated and wild-type fish. These fish presented with less organized and significantly less statoacoustic neurons when compared with mock-treated fish (36.0 ± 6.4 versus 52.3 ± 8 neurons, $P = 0.01$) and wild-type fish (51.5 ± 2.1 , $P = 0.02$) (Fig. 4C and D). In addition, *usp48* crispants showed a significant delay in the development of primary motor neurons at 28 hpf that got exacerbated at 48 hpf (Supplementary Material, Fig. S7). During early development, the size of 1 dpf *usp48* knocked-down embryos was smaller when compared with that of mock-treated and wild-type animals ($P = 0.02$) (Supplementary Material, Fig. S8). The subsequent development of the swim-bladder, a double-chambered organ located in the coelom used to maintain buoyancy that may also function as an acoustic resonator appeared slower in treated fish (data not shown), suggesting a general delay in the development of *usp48* knock-downs.

Discussion

We describe three families with ADNSHHL. The affected individuals of the first two families presented with bilateral hearing loss and heterozygosity of predicted-to-be deleterious missense variants in the ubiquitin carboxyl-terminal hydrolase USP48, while the affected individual of the third family exhibited unilateral cochlear aplasia-associated hearing loss and a *de novo* splicing variant in the same gene. Whereas further cases are warranted to demonstrate if a single or multiple pathological processes are associated with missense and truncation variants, we showed that the Italian, Dutch and French variants impair the enzymatic activity of the encoded enzyme and that zebrafish ablated for the orthologous *usp48* are hearing impaired. Altogether, these data and the observation that there is a significant paucity of USP48 truncation variants in the human population suggest haploinsufficiency as mechanism of action. Of note, the phenotypic variability among the affected individuals of the Italian family cannot be explained by the presence of more than one genetic cause of hearing loss as the targeted screening of variants in the commonest 99 deafness genes was negative.

We observed expression of USP48 in the human fetal SG and Scarpa's neurons, as well as a general developmental delay of the neuronal system of *usp48* knocked-down zebrafish. These crispants presented with significantly less statoacoustic neurons and a decreased ASR suggesting that the USP48-encoded ubiquitin carboxyl-terminal hydrolase is important to auditory function. USP48 also controls the E3 ubiquitin-protein ligase Mdm2 (25) (MIM: 164785), which ubiquitinates and antagonizes p53 (MIM: 191170). USP48 role in controlling DNA repair is further highlighted by its function as a histone H2A deubiquitinase that counteracts BRCA1 E3 ubiquitin-ligase activity (26) (breast cancer 1; MIM: 113705) and by the reduced chromosomal instability of Fanconi anemia cells upon knock-down of USP48 (27,28). USP48 was also shown to regulate the stability of TRAF2 (tumor necrosis factor receptor-associated factor 2; MIM: 601895), thus controlling E-cadherin-mediated adherens junctions. Such junctions are important for cochlear development and growth of auditory neurons (29). The expression level of E-cadherin is determinant for hair cell differentiation; its level inversely correlates to the capacity of SCs to differentiate into sensory hair cells (30). Data suggest that in the absence of sound, developing cochlear and primary auditory neurons undergo experience-independent activity. Two hypotheses were suggested for this activity: the inner SCs of the Kölliker's organ, an organ only present during the critical period of auditory development, release ATP hence

recapitulating auditory neuron activity or alternatively inner hair cells (IHCs) generate this spontaneous activity without ATP activation (22,31). Nevertheless, it was proposed that 'developmental abnormalities of the Kölliker's organ may lead to congenital hearing loss as mutations in ion channels important for its activity (e.g. *GJB2*, *GJB6*) are associated with deafness' (22). Whereas E-cadherin is present in OHCs, it is not expressed in IHCs or in the part of the Kölliker's organ in contact with them. We similarly observe expression of USP48 in the Kölliker's organ, but not in the developing IHCs.

In conclusion, we have identified a new ADNSHHL candidate gene. Our results support adding USP48 to the list of genes associated with hearing function and to future HHL diagnostic panels. Our findings also emphasize the importance of the temporary Kölliker's organ in auditory development.

Materials and Methods/Ethical Approval

Each participant signed consent forms for clinical studies. In Italy, the research approval was obtained from the Institutional Review Board of IRCCS Burlo Garofolo, Trieste. The study of the Dutch subject was approved by the medical ethics committee of the Radboudumc (registration number: NL33648.091.10). The research was conducted according to the ethical standards defined by the Helsinki Declaration.

Use of human fetal specimens was in accordance with the Dutch legislation (Fetal Tissue Act, 2001) and the WMA Declaration of Helsinki guidelines. Approval was obtained from the Medical Research Ethics Committee of Leiden University Medical Center (protocol registration number B18.044). Written informed consent of the donors was obtained following the Guidelines on the Provision of Fetal Tissue set by the Dutch Ministry of Health, Welfare and Sport (revised version, 2018).

Clinical description

The hearing loss is defined by World Health Organization (WHO) as a speech-frequency pure tone average > 25 dB at 500, 1000, 2000 and 4000 Hz in the better hearing ear (32). In particular, disabling deafness is described as loss of auditory ability > 40 dB in adults and > 30 dB in children, in the better hearing ear (see who.int/news-room/fact-sheets/detail/deafness-and-hearing-loss). Deafness can be classified in different degrees from mild (26–40 dB), moderate (41–dB), moderately severe (56–70 dB), severe (71–90 dB) up to profound hearing loss (≥ 91 dB) (33).

All NSHHL living affected individuals of the Italian family underwent a clinical ENT examination. Hearing function was assessed by pure-tone audiometry, tympanogram and otoacoustic emissions (Supplementary Material, Fig. S1). Other clinical tests were carried out to exclude syndromic forms. The French proband is the second child of unrelated parents of French origin without any familial medical history (Guyana and French metropolis). She was born at term (38 + 3 GW) from a dizygotic twin pregnancy with normal weight (2830 g), length (46 cm) and head circumference (33 cm). She had good psychomotor development, sitting at 6 months, walking at 16 months.

Genetic analyses

Italian family. DNA was extracted from peripheral blood using a QIAasympy instrument (Qiagen, Hilden, Germany) and quantified with a Nanodrop ND-1000 spectrophotometer (NanoDrop Technologies, Olching, Germany). The family was sequentially assessed for causative variants in *GJB2* (MIM: 121011), *GJB6* (MIM:

604418), MTRNR1 (MIM: 561000) and a panel of 96 deafness genes by targeted resequencing (34) with negative results. ES was performed using the Ion Proton™ platform according to the manufacturer's protocols (Life Technologies, Monza MB, Italy). Briefly, 1 µg of genomic DNA was used to construct DNA libraries using the Ion AmpliSeq™ Exome Kit. The overall mean-depth base coverage was 102-fold, while on average, 89% of the targeted region was covered at least 20-fold. Read mapping and variant calling were performed using Ion Torrent Suite v4.0 software (Life Technologies, Monza MB, Italy). Variants were filtered using Varapp according to the quality of the calling, their frequency in control populations ($\leq 1\%$ in 1000 genome and Genome Aggregation Database (GnomAD) v2.1.1) and their predictive impact on the function of the protein (high and medium impact in PolyPhen-2 and SIFT databases, GERP score ≥ 3.00 and CADD (scaled) ≥ 10.00) as described (35) and an autosomal dominant inheritance scenario. Sanger sequencing was used to confirm segregation.

Dutch proband. Exome capture, sequencing and variant filtering was performed as previously described in particular no likely pathogenic variant was identified in a list of 156 known deafness genes (36).

French proband. DNA was extracted from leucocytes from the proband and her parents. An array-CGH (400 kb resolution) was normal. Exome capture was performed with the Sure Select Human All Exon kit (Agilent Technologies, Les Ulis, France). Agilent Sure Select Human All Exon (58 Mb, V6) libraries were prepared from 3 µg of genomic DNA sheared with an Ultrasonicator (Covaris, Woburn, USA) as recommended by the manufacturer. Barcoded exome libraries were pooled and sequenced with an HiSeq2500 system (Illumina, Évry-Courcouronnes, France), generating paired-end reads. After demultiplexing, sequences were mapped on the human genome reference (NCBI build 37, hg19 version) with BWA. Variant calling was carried out with the Genome Analysis Toolkit (GATK), SAMtools and Picard tools. Single-nucleotide variants were called with GATK Unified Genotyper, whereas indel calls were made with the GATK IndelGenotyper_v2. All variants with a read coverage $\leq 2\times$ and a Phred-scaled quality ≤ 20 were filtered out. The overall mean-depth base coverage of the trio was between 142- and 217-fold, while more than 99% of the targeted region was covered at least 15-fold. Variant-filtering strategies especially familial segregation led to the identification of only one candidate variant: a *de novo* affecting a splice donor site in USP48.

Ubiquitin hydrolase activity assay

The plasmids pcDNA3 expressing hUSP48 wild-type (FLAG-USP48^{WT}; ENST00000308271.14) and a catalytically dead enzyme (FLAG-USP48^{C98S}) were donated by Dr G. Mosialos, Aristotle University of Thessaloniki (37). The USP48 mutations identified in the Italian, French and Dutch probands were engineered using the QuikChange II XL Site-Directed Mutagenesis Kit (Agilent Technologies, Basel, Switzerland) following the manufacturer's instructions. The FLAG-USP48¹⁻¹⁰¹⁹ encoding a truncated protein was engineered by site-directed mutagenesis of the Gln1019 CAA codon into an ochre TAA stop codon. Sanger sequencing confirmed each variant. HEK293T cells were transfected with FuGene (FuGene Hd Transfection, #E2312, Promega, Dübendorf, Switzerland). Cells were cultured at 37°C under 2–4% CO₂ in DMEM supplemented with 10% FBS and 1% Pen/Strep. Cells were lysed 24 or 48 h after the transient transfection in RIPA

buffer (#20–188, Millipore, Darmstadt, Germany) supplemented with proteases inhibitors (Halt Protease & Phosphatase inhibitor cocktail, #78440, Thermo Scientific, Zürich, Switzerland). The protein lysate concentration was determined by BCA Assay (Pierce, BCA Protein Assay Kit #23227, Thermo Scientific, Zürich, Switzerland). Equal amounts of proteins were resolved on 4–15% SDS-PAGE mini-gels and transferred to nitrocellulose membranes (GE Healthcare, Life Science, Dornstadt, Germany) to assess FLAG-USP48 expression. Immunoblots were blocked in 5% milk powder in TBST (50 mM Tris-HCl, pH 7.4, 200 mM NaCl and 0.1% Tween 20) for 1 h at room temperature (RT). Membranes were incubated overnight at +4°C with primary antibodies: anti-Flag 1:20000 (#F3165, anti-Mouse, Sigma, Zurich, Switzerland) and anti- α -actin 1:2500 (anti-Rabbit, Sigma, Zurich, Switzerland) diluted in TBST. Secondary antibodies: anti-Mouse-HRP (#W402B, Promega, Dübendorf, Switzerland) and anti-Rabbit-HRP (#sc-2030, Santa Cruz Biotechnology, Heidelberg, Germany) were diluted, 1:2500 and 1:5000, respectively, in TBST and incubated for 1 h at RT. Reactive bands were detected with ECL detection kit (Immobilon Western Kit, Millipore, Darmstadt, Germany). Ubiquitin hydrolase activity assay were performed as described (37). Briefly, wild-type or mutated FLAG-tagged USP48 proteins were immunoprecipitated from cell lysates without protease inhibitors 48 h post-transfection. Immunoprecipitated proteins were incubated with 0.8/1 µg of tetraubiquitin molecules (63-linked polyubiquitin chain, Boston Biochem, Boston, USA). Reactions were separated by SDS-PAGE followed by Coomassie staining.

Protein model

A USP7 (MIM: 602519) model was built using Swiss-PdbViewer (spdbv) (38) as described (39). The chain C of pdb entry 4YOC (40) was superposed onto pdb entry 5J7T using the iterative magic fit function of spdbv. Residues Phe787 and onward of 5J7T were deleted and replaced by residues Phe787-Gly1078 of 4YOC chain C, which was renamed to chain A. The structure of USP9X (MIM: 300072; pdb entry 5WCH) (41) was then superposed onto the model of USP7; the backbone of pdb entry 5WCH chain A residues Arg1896-Cys1908 and Ala1948-Arg1955 were superposed onto the corresponding residues of the USP7 model (residues Lys476-Cys488 and Ala513-Arg520). Finally, the USP48 sequence (Swiss-Prot entry Q86UV5) was aligned onto the USP7 template.

Human inner ear expression

Human fetal inner ears were collected after elective termination of pregnancy by vacuum aspiration. Fetal age (in weeks, W), defined as the duration since fertilization, was determined by obstetric ultrasonography prior to termination. Tissue was obtained at the following developmental stages: W12 (n=3), W14 (n=3), W15 (n=2), W16 (n=2) and W17 (n=1). Inner ears were fixed in 4% paraformaldehyde, decalcified and embedded in paraffin as previously described (42). Sections (5 µm) were cut using an HM 355 S rotary microtome (Thermo Fisher Diagnostics, Darmstadt, Germany). Sections were deparaffinized in xylene and rehydrated, followed by standard immunohistochemistry procedure (42). Sections were incubated overnight at +4°C with a monoclonal mouse anti-USP48 antibody (1:10, #H00084196-M01, Abnova, Heidelberg, Germany). Next, sections were incubated with a secondary AF594 donkey anti-mouse antibody (1:500, #A-21203, Thermo Fisher Scientific, Frankfurt am Main, Germany) for 1 h at RT. Nuclei were stained with DAPI. Negative controls were carried out by matching isotype controls and omitting

primary antibodies. Positive controls were carried out by conducting isotype control experiments on fetal inner ears (Mouse IgG Isotype Control, #08–6599, Invitrogen, Merelbeke, Belgium). In addition, to compensate for any aspecific binding of secondary antibodies, primary antibodies were omitted. Lastly, positive controls were carried out by staining sections of known positive human tissue samples. Images of these negative controls are presented in [Supplementary Material, Fig. S3](#). At least, three separate immunostaining experiments for each fetal stage were performed.

Zebrafish model

Zebrafish (*Danio rerio*, Oregon AB) were maintained at 28.5°C and on a 14:10 h light/dark cycle and staged by hours (h) or days (d) post-fertilization (pf). Eggs were obtained by random mating between sexually mature animals. All procedures complied with both the European Convention for the Protection of Animals used for Experimental and Scientific Purposes and the National Institutes of Health guide for the care and use of Laboratory animals. Housing and experiments were approved by the local authorities, i.e. the Vaud cantonal authority (authorization VD-H21) and INSERM, Montpellier University. We generated founder F0 mutant zebrafish depleted for *usp48* by CRISPR/Cas9 genome editing. Three distinct guide (g)RNAs targeting coding sequence in *usp48* exon 4 (*gusp48-4* 5'-AGATGCTCGCAAATCGTCCGTGG-3'), exon 9 (*gusp48-9* 5'-AGCGCGGTGTTGATTCATCG-3') and exon 10 (*gusp48-10* 5'-GACAGAAGAGATTAACCAGA-3') were designed using the CHOPCHOP tool (43). The targeted exons are present in the three different *usp48* transcripts annotated by Ensembl (Zebrafish GRCz11). Briefly, gRNAs were transcribed *in vitro* using the GenArt gRNA synthesis kit (#A29377, ThermoFisher, Frankfurt am Main, Germany) according to the manufacturer's instructions. A total of 1 nl of a cocktail containing 100 ng/μl of each gRNA was injected with 200 ng/μl of Cas9 protein (PNA Bio, Thousand Oaks, USA), as treatment, or with the same amount (μl) of water, as control, was injected into one-cell stage embryos. KCl (200 mM) was added to increase the efficiency of the method and Phenol-Red (4×) to visualize the injection. Toxicity of the three guides was compared at 48 hpf, while their efficacy was assessed after 72 hpf analyzing fish locomotion. To determine targeting efficiency in founder (F0) mutants, we extracted genomic DNA from 2 dpf embryos and PCR amplified the region flanking the gRNA target site. PCR products were denatured, reannealed slowly and separated on a 20% TBE 1.0 mm precast polyacrylamide gel (Thermo Fisher Scientific, Frankfurt am Main, Germany), which was then incubated in ethidium bromide and imaged on a ChemiDoc system (Bio-Rad, Hercules, CA) to visualize hetero- and homoduplexes. Targeting efficiency in founder (F0) mutants was also assessed in 5dpf embryos by T7 assay. Briefly, DNA was extracted, and PCR amplified with primers flanking the gRNA target site (5'-CGGACGATTTGCGAGCATCT-3'). PCR products were denatured, reannealed and separated on an agarose gel allowing to assess rearrangements at the targeted site ([Supplementary Material, Fig. S9](#)).

Locomotion assays

A first qualitative analysis was performed exploiting the touch-response test on 72 hpf larvae, by a slight touch stimulation. The motion of each single larva was examined and scored as « normal swimming », « motionless », « looping swimming » or « pinwheel swimming ». Representative tracking video was obtained with a camera. A second quantitative test was performed analyzing 5 dpf zebrafish spontaneous motility using

the ZebraBox® recording system (Viewpoint, Lissieu, France). Locomotion was recorded for each individual larva on a 96-well plate for 10/15 min and presented as slow (3–6 mm/s) and high velocities (>6 mm/s) (44).

Acoustic startle response

Five dpf zebrafish larvae were transferred to a 96-well plate in 300 μl of water per well and then placed in a ZebraBox® (ViewPoint, Lissieu, France) inside a soundproof box. After 30 min of adaptation, larvae were exposed to three intermittent noise stimulations, 1 s per stimulus. Several frequencies were assessed at 90 dB: 400, 600, 800, 1000 Hz and a broad-band noise, a.k.a. white noise, consisting of all frequencies together. The experiments were performed in light condition. The noise was computer-generated and played through two commercial aerial loudspeakers placed in the chamber. The sound intensity within the box was measured with a noise detector. The variation in ASR was quantified to assess hearing ability. The activity of larvae was automatically and objectively measured before and after sound stimuli and then analyzed. Zebrafish activity was quantified using the quantization mode of ZebraLab® software (Viewpoint, Lissieu, France) (45). The results were pooled into 1 s time bins to assess ASR.

Visual motor response

Five dpf zebrafish larvae were transferred to a 96-well plate and then placed inside a ZebraBox® (ViewPoint, Lissieu, France) equipped with infrared illumination for imaging in the dark itself positioned in a soundproof box. In the box, white light can be controlled accurately. The light–dark protocol consisted of 30 min of adaptation in the dark followed by two alternating periods of light (100% of light intensity) and dark of 10 min each one. Zebrafish activity was quantified using the ZebraLab® software (Viewpoint, Lissieu, France) (45). Data were pooled into 1 min time bins to assess the VMR.

Statistics

Differences between experimental groups were determined by the GraphPad Prism software (version 8.0). Student's *t*-tests (two-tailed) were performed to analyze behavioral changes in response to noise and light stimulation. The minimum criterion for significance was $P < 0.05$.

Immunohistochemistry of Zebrafish embryos

Zebrafish were treated with 75 μM PTU (1-phenyl 2-thiourea) from 24 hpf to prevent pigmentation. Zebrafish analyzed at 28 hpf were dechorionated before fixation. At appropriate developmental stages, they were anesthetized with 0.0168% tricaine (MS-222, E1052, Sigma-Aldrich, Zürich, Switzerland) and fixed in 4% PFA for 1 h at RT, permeabilized first in 1× phosphate saline buffer (PBS), 0.5% Triton X-100, for 90 min and subsequently in 1X PBS, 1%Triton X-100, for 2 h on a shaker. Embryos were incubated in blocking buffer (1% BSA in 1× PBS) for 1 h at RT and incubated in primary antibodies overnight at 4°C on a shaker. Primary antibodies were from following sources: mouse anti-synaptotagmin 2 (Znp-1, 1:100, DSHB), mouse anti-islet 1 and 2 (39.4D5, 1:100, DSHB) and anti-α-bungarotoxin Alexa Fluor™ 555 conjugate (B35451, 1:50, Invitrogen, Merelbeke, Belgium). Following washes with 1× PBS, the embryos were incubated in secondary antibodies overnight at 4°C. For immunofluorescence: Alexa Fluor™ 488 conjugated secondary antibody (1:500) and Phalloidin (1:2000) were used. Nuclei were stained with

DAPI (1:8000) for 10 min at RT. Imaging was performed using confocal microscope LSM880 airyscan (Carl Zeiss, Oberkochen, Germany). Quantification of motor neurons projection lengths was obtained with ImageJ software.

Otoliths, hair cells and statoacoustic neuron structures in Zebrafish larvae

Zebrafish larvae were analyzed at different timepoints to compare the phenotype and the morphology of specialized structures among treated, controls and wild-type fish. Eggs were obtained by random mating between sexually mature animals (AB line). Some were fixed with PFA 4% in 1× PBS to assess the distance and dimension of otoliths at 5 dpf, and the morphological phenotype during development from 1 to 5 dpf. Eggs imaging was performed using an optical microscope. Fish length was measured from the head side of the swim bladder to the end of the tail from 3 dpf onwards. Fish length corresponded to the entire animal length from head to tail at 1 and 2 dpf. Other eggs were anesthetized with 0.0168% tricaine (MS-222, E1052, Sigma-Aldrich, Zürich, Switzerland), bathed in 2 μM of YO-PRO-1 for 30 min, followed by three washes with 1× PBS, to assess the functionality of the hair cells at 3 and 5 dpf. Imaging was performed using a fluorescent microscope (Olympus, Lausanne, Switzerland). A third group of eggs obtained by mating Brn3c:mGFP females in which hair cells of the inner ear and the lateral line neuromasts are specifically labelled in green (46) and NBT-dsRED males in which the neuronal system is labelled in red (neural-specific beta tubulin promoter driving expression of dsRed red fluorescent protein (47)) were anesthetized with 0.0168% tricaine and analyzed at 3, 4 and 5 dpf to assess the structure of the hair cells and statoacoustic neurons expressed in the ear. Imaging was performed using confocal microscope LSM880 airyscan (Carl Zeiss, Oberkochen, Germany).

Web Resources

ChopChop design tool: <http://chopchop.cbu.uib.no>
 gEAR portal: <https://umgear.org/#1>
 Genome Browser: <https://genome.ucsc.edu/>
 GnomAD: <https://gnomad.broadinstitute.org/>
 MaxEntScan: http://hollywood.mit.edu/burgelab/maxent/Xmaxentscan_scoreseq.html
 NNSplice: https://www.fruitfly.org/seq_tools/splice.html
 OMIM (Online Mendelian Inheritance in Man): <http://www.omi.org>
 The Human Protein ATLAS: <https://www.proteinatlas.org/>
 WHO Deafness and hearing loss: https://www.who.int/health-topics/hearing-loss#tab=tab_1

Supplementary Material

Supplementary Material is available at HMG online.

Acknowledgements

We thank the affected individuals and their families for their participation in this study. We are grateful to Jacques S. Beckmann for comments. We are indebted to the zebrafish facility and the cell imaging facility of the University of Lausanne and the Montpellier ZebraSens behavioral phenotyping platform (MMDN) in particular to N. Cubedo and J. Sarniguet for help. The Dutch DOOFNL Consortium consisting of M.F. van Dooren, S.G. Kant, H.H.W. de Gier, E.H. Hoefsloot, M.P. van der Schroeff, L.J.C.

Rotteveel, F.G. Ropers, J.C.C. Widdershoven, J.R. Hof, E.K. Vanhoutte, I. Feenstra, H. Kremer, C.P. Lanting, R.J.E. Pennings, H.G. Yntema, R.H. Free and J.S. Klein Wassink-Ruiter, R.J. Stokroos, A.L. Smit, M.J. van den Boogaard, F.A. Ebbens, S.M. Maas, A. Plomp, T.P.M. Goderie, P. Merkus and J. van de Kamp, contributed to the clinical evaluation and medical genetic testing of a cohort of ~800 genetically unsolved index cases with hearing loss, evaluated for USP48 variants. S.B. is recipient of scholarships from the European Social Fund, University of Trieste, Italy and the Fund for Research and Education in Genetics, University of Lausanne, Switzerland.

Conflict of Interest statement. The authors declare no conflict of interest.

Funding

Swiss National Science Foundation (31003A_182632 to A.R. and 320030_170062 and 188789 to F.A.); Horizon2020 Twinning project ePerMed (692145) to A.R.; Heinsius-Houbolt foundation to H.K. The funders had no role in study design, data collection and analysis, decision to publish or preparation of the manuscript.

Authors' Contribution

G.G. and A.R. conceived and directed the study. S.B., A.M., N.C., M.C., F.F., R.M., S.P., J.J.S., J.M.v.d.K., A.Z., S.M., H.K., P.G., G.G. and A.R. recruited patients, gathered clinical information, prepared samples, performed whole-exome and mutational analysis. S.B., M.R., N.V., Y.A., B.D., F.A. and T.M. engineered and phenotyped the zebrafish model. E.v.B. and H.L. performed the immunohistochemistry. S.B., J.C. and G.G. carried out the other experiments. N.G. performed structural modeling of variants. S.B. performed statistical analysis and analyzed the data. S.B. and A.R. wrote the manuscript. All authors reviewed and approved the manuscript.

References

1. Kremer, H. (2019) Hereditary hearing loss; about the known and the unknown. *Hear. Res.*, **376**, 58–68.
2. Azaiez, H., Booth, K.T., Ephraim, S.S., Crone, B., Black-Ziegelbein, E.A., Marini, R.J., Shearer, A.E., Sloan-Heggen, C.M., Kolbe, D., Casavant, T. et al. (2018) Genomic landscape and mutational signatures of deafness-associated genes. *Am. J. Hum. Genet.*, **103**, 484–497.
3. Morgan, A., Koboldt, D.C., Barrie, E.S., Crist, E.R., Garcia Garcia, G., Mezzavilla, M., Faletra, F., Mihalic Mosher, T., Wilson, R.K., Blanchet, C. et al. (2019) Mutations in PLS1, encoding fimbrin, cause autosomal dominant nonsyndromic hearing loss. *Hum. Mutat.*, **40**, 2286–2295.
4. Eaton, R.C. and Didomenico, R. (1986) Role of the teleost escape response during development. *Trans. Am. Fish. Soc.*, **115**, 128–142.
5. Zeddies, D.G. and Fay, R.R. (2005) Development of the acoustically evoked behavioral response in zebrafish to pure tones. *J. Exp. Biol.*, **208**, 1363–1372.
6. Riley, B.B. and Moorman, S.J. (2000) Development of utricular otoliths, but not saccular otoliths, is necessary for vestibular function and survival in zebrafish. *J. Neurobiol.*, **43**, 329–337.
7. Busch-Nentwich, E., Sollner, C., Roehl, H. and Nicolson, T. (2004) The deafness gene *dfna5* is crucial for *ugdh* expression and HA production in the developing ear in zebrafish. *Development*, **131**, 943–951.

8. Kazmierczak, M., Harris, S.L., Kazmierczak, P., Shah, P., Starovoytov, V., Ohlemiller, K.K. and Schwander, M. (2015) Progressive hearing loss in mice carrying a mutation in *Usp53*. *J. Neurosci.*, **35**, 15582–15598.
9. Yokoyama, J.S., Lam, E.T., Ruhe, A.L., Erdman, C.A., Robertson, K.R., Webb, A.A., Williams, D.C., Chang, M.L., Hytonen, M.K., Lohi, H. et al. (2012) Variation in genes related to cochlear biology is strongly associated with adult-onset deafness in border collies. *PLoS Genet.*, **8**, e1002898.
10. Shimada, A., Ebisu, M., Morita, T., Takeuchi, T. and Umemura, T. (1998) Age-related changes in the cochlea and cochlear nuclei of dogs. *J. Vet. Med. Sci.*, **60**, 41–48.
11. Ghanem, A., Schweitzer, K. and Naumann, M. (2019) Catalytic domain of deubiquitinylase USP48 directs interaction with Rel homology domain of nuclear factor kappaB transcription factor RelA. *Mol. Biol. Rep.*, **46**, 1369–1375.
12. Lang, H., Schulte, B.A., Zhou, D., Smythe, N., Spicer, S.S. and Schmiedt, R.A. (2006) Nuclear factor kappaB deficiency is associated with auditory nerve degeneration and increased noise-induced hearing loss. *J. Neurosci.*, **26**, 3541–3550.
13. Kaplanis, J., Samocho, K.E., Wiel, L., Zhang, Z., Arvai, K.J., Eberhardt, R.Y., Gallone, G., Lelieveld, S.H., Martin, H.C., McRae, J.F. et al. (2020) Evidence for 28 genetic disorders discovered by combining healthcare and research data. *Nature*, **586**, 757–762.
14. Tatsi, C. and Stratakis, C.A. (2019) The Genetics of Pituitary Adenomas. *J. Clin. Med.*, **9**(1), 30.
15. Chen, J., Jian, X., Deng, S., Ma, Z., Shou, X., Shen, Y., Zhang, Q., Song, Z., Li, Z., Peng, H. et al. (2018) Identification of recurrent USP48 and BRAF mutations in Cushing's disease. *Nat. Commun.*, **9**, 3171.
16. Uddin, M., Tammimies, K., Pellecchia, G., Alipanahi, B., Hu, P., Wang, Z., Pinto, D., Lau, L., Nalpathamkalam, T., Marshall, C.R. et al. (2014) Brain-expressed exons under purifying selection are enriched for de novo mutations in autism spectrum disorder. *Nat. Genet.*, **46**, 742–747.
17. Elliott, P.R., Liu, H., Pastok, M.W., Grossmann, G.J., Rigden, D.J., Clague, M.J., Urbe, S. and Barsukov, I.L. (2011) Structural variability of the ubiquitin specific protease DUSP-UBL double domains. *FEBS Lett.*, **585**, 3385–3390.
18. Clerici, M., Luna-Vargas, M.P., Faesen, A.C. and Sixma, T.K. (2014) The DUSP-Ubl domain of USP4 enhances its catalytic efficiency by promoting ubiquitin exchange. *Nat. Commun.*, **5**, 5399.
19. Zimmermann, L., Stephens, A., Nam, S.Z., Rau, D., Kubler, J., Lozajic, M., Gabler, F., Soding, J., Lupas, A.N. and Alva, V. (2018) A completely reimplemented MPI bioinformatics toolkit with a new HHpred server at its core. *J. Mol. Biol.*, **430**, 2237–2243.
20. Blom, N., Sicheritz-Ponten, T., Gupta, R., Gammeltoft, S. and Brunak, S. (2004) Prediction of post-translational glycosylation and phosphorylation of proteins from the amino acid sequence. *Proteomics*, **4**, 1633–1649.
21. Ryals, M., Pak, K., Jalota, R., Kurabi, A. and Ryan, A.F. (2017) A kinase inhibitor library screen identifies novel enzymes involved in ototoxic damage to the murine organ of Corti. *PLoS One*, **12**, e0186001.
22. Dayaratne, M.W., Vlajkovic, S.M., Lipski, J. and Thorne, P.R. (2014) Kolliker's organ and the development of spontaneous activity in the auditory system: implications for hearing dysfunction. *Biomed. Res. Int.*, **2014**, 367939.
23. Vona, B., Doll, J., Hofrichter, M.A.H., Haaf, T. and Varshney, G.K. (2020) Small fish, big prospects: using zebrafish to unravel the mechanisms of hereditary hearing loss. *Hear. Res.*, **397**, 107906.
24. Kindt, K.S. and Sheets, L. (2018) Transmission disrupted: modeling auditory synaptopathy in zebrafish. *Front. Cell Dev. Biol.*, **6**, 114.
25. Cetkovska, K., Sustova, H. and Uldrijan, S. (2017) Ubiquitin-specific peptidase 48 regulates Mdm2 protein levels independent of its deubiquitinase activity. *Sci. Rep.*, **7**, 43180.
26. Uckelmann, M., Densham, R.M., Baas, R., Winterwerp, H.H.K., Fish, A., Sixma, T.K. and Morris, J.R. (2018) USP48 restrains resection by site-specific cleavage of the BRCA1 ubiquitin mark from H2A. *Nat. Commun.*, **9**, 229.
27. Truty, R., Paul, J., Kennemer, M., Lincoln, S.E., Olivares, E., Nussbaum, R.L. and Aradhya, S. (2019) Prevalence and properties of intragenic copy-number variation in Mendelian disease genes. *Genet. Med.*, **21**, 114–123.
28. Velimezi, G., Robinson-Garcia, L., Munoz-Martinez, F., Wiegant, W.W., Ferreira da Silva, J., Owusu, M., Moder, M., Wiedner, M., Rosenthal, S.B., Fisch, K.M. et al. (2018) Map of synthetic rescue interactions for the Fanconi anemia DNA repair pathway identifies USP48. *Nat. Commun.*, **9**, 2280.
29. Wang, B., Hu, B. and Yang, S. (2015) Cell junction proteins within the cochlea: a review of recent research. *J. Otolaryngol.*, **10**, 131–135.
30. Collado, M.S., Thiede, B.R., Baker, W., Askew, C., Igbani, L.M. and Corwin, J.T. (2011) The postnatal accumulation of junctional E-cadherin is inversely correlated with the capacity for supporting cells to convert directly into sensory hair cells in mammalian balance organs. *J. Neurosci.*, **31**, 11855–11866.
31. Wang, H.C. and Bergles, D.E. (2015) Spontaneous activity in the developing auditory system. *Cell Tissue Res.*, **361**, 65–75.
32. Yamasoba, T., Lin, F.R., Someya, S., Kashio, A., Sakamoto, T. and Kondo, K. (2013) Current concepts in age-related hearing loss: epidemiology and mechanistic pathways. *Hear. Res.*, **303**, 30–38.
33. Koffler, T., Ushakov, K. and Avraham, K.B. (2015) Genetics of hearing loss: syndromic. *Otolaryngol. Clin. N. Am.*, **48**, 1041–1061.
34. Vozzi, D., Morgan, A., Vuckovic, D., D'Eustacchio, A., Abdulhadi, K., Rubinato, E., Badii, R., Gasparini, P. and Giroto, G. (2014) Hereditary hearing loss: a 96 gene targeted sequencing protocol reveals novel alleles in a series of Italian and Qatari patients. *Gene*, **542**, 209–216.
35. Gueneau, L., Fish, R.J., Shamseldin, H.E., Voisin, N., Tran Mau-Them, F., Preiksaitiene, E., Monroe, G.R., Lai, A., Putoux, A., Allias, F. et al. (2018) KIAA1109 variants are associated with a severe disorder of brain development and arthrogryposis. *Am. J. Hum. Genet.*, **102**, 116–132.
36. Smits, J.J., Oostrik, J., Beynon, A.J., Kant, S.G., de Koning Gans, P.A.M., Rotteveel, L.J.C., Klein Wassink-Ruiter, J.S., Free, R.H., Maas, S.M., van de Kamp, J. et al. (2019) De novo and inherited loss-of-function variants of ATP2B2 are associated with rapidly progressive hearing impairment. *Hum. Genet.*, **138**, 61–72.
37. Tzimas, C., Michailidou, G., Arsenakis, M., Kieff, E., Mosialos, G. and Hatzivassiliou, E.G. (2006) Human ubiquitin specific protease 31 is a deubiquitinating enzyme implicated in activation of nuclear factor-kappaB. *Cell. Signal.*, **18**, 83–92.
38. Nicolas Guex, M.C.P. (1997) <SWISS-MODEL and the Swiss-PdbViewer- an environment for comparative protein modeling>. *Electrophoresis*, **15**, 2714–2723.

39. Rouge, L., Bainbridge, T.W., Kwok, M., Tong, R., Di Lello, P., Wertz, I.E., Maurer, T., Ernst, J.A. and Murray, J. (2016) Molecular understanding of USP7 substrate recognition and C-terminal activation. *Structure*, **24**, 1335–1345.
40. Cheng, J., Yang, H., Fang, J., Ma, L., Gong, R., Wang, P., Li, Z. and Xu, Y. (2015) Molecular mechanism for USP7-mediated DNMT1 stabilization by acetylation. *Nat. Commun.*, **6**, 7023.
41. Paudel, P., Zhang, Q., Leung, C., Greenberg, H.C., Guo, Y., Chern, Y.H., Dong, A., Li, Y., Vedadi, M., Zhuang, Z. et al. (2019) Crystal structure and activity-based labeling reveal the mechanisms for linkage-specific substrate recognition by deubiquitinase USP9X. *Proc. Natl. Acad. Sci. U. S. A.*, **116**, 7288–7297.
42. Locher, H., Frijns, J.H.M., van Iperen, L., de Groot, J.C.M.J., Huisman, M.A. and de Sousa Lopes, S.M.C. (2013) Neurosensory development and cell fate determination in the human cochlea. *Neural Dev.*, **8**, 20.
43. Labun, K., Montague, T.G., Gagnon, J.A., Thyme, S.B. and Valen, E. (2016) CHOPCHOP v2: a web tool for the next generation of CRISPR genome engineering. *Nucleic Acids Res.*, **44**, W272–W276.
44. Arribat, Y., Mysiak, K.S., Lescouzeres, L., Boizot, A., Ruiz, M., Rossel, M. and Bomont, P. (2019) Sonic hedgehog repression underlies gigaxonin mutation-induced motor deficits in giant axonal neuropathy. *J. Clin. Invest.*, **129**, 5312–5326.
45. Liu, X., Lin, J., Zhang, Y., Guo, N. and Li, Q. (2018) Sound shock response in larval zebrafish: a convenient and high-throughput assessment of auditory function. *Neurotoxicol. Teratol.*, **66**, 1–7.
46. Di Donato, V., Auer, T.O., Duroure, K. and Del Bene, F. (2013) Characterization of the calcium binding protein family in zebrafish. *PLoS One*, **8**, e53299.
47. Peri, F. and Nusslein-Volhard, C. (2008) Live imaging of neuronal degradation by microglia reveals a role for v0-ATPase a1 in phagosomal fusion in vivo. *Cell*, **133**, 916–927.